ELSEVIER

Journal of Chromatography B, 743 (2000) 431–441

JOURNAL OF CHROMATOGRAPHY B

www.elsevier.com/locate/chromb

Cold cataracts: a naturally occurring aqueous two-phase system

Paul Petitt, Daniel Forciniti*

Chemical Engineering Department, University of Missouri-Rolla, Rolla MO 65409, USA

Abstract

The cytoplasm of the eye lenses shows a liquid–liquid phase transition similar to the one observed in aqueous two-phase systems. This phenomenon is known as cold cataracts. We have studied the solution behavior of the main protein fractions that constitute the lenses' cytoplasm using small-angle neutron scattering and dynamic light scattering. Our results provide evidence that an intricate balance of forces underlines the physical phenomena responsible for the optical properties of the lenses and for the phase transition that is observed as the temperature is lowered below some critical value. These forces include solvent-mediated forces besides the more conventional Coulombic and dispersion forces. This study suggests that solvent mediated forces must be included to successfully model liquid–liquid phase transitions like the ones observed in cold cataracts or in aqueous two-phase systems.

Keywords: Aqueous two-phase systems; Cold cataracts

1. Introduction

Aqueous two phase systems refers to a variety of two liquid phases at equilibrium where either one or both phases are mostly water. Usually, aqueous two-phase systems are made up of two polymers and water or one polymer, salt and water [1]. It has been known for quite sometime, however, that even proteins at high concentrations produce aqueous two-phase systems [2]. A naturally occurring one is the aqueous two-phase system formed in the eye lenses when the temperature is lowered below some critical value. This phenomenon is known as cold-cataracts [3–7].

In cold cataracts the lenses' cytoplasm separates into a protein-rich phase and a protein-poor phase because the proteins present in the lenses' cytoplasm exhibit a solubility gap with an upper consolute point. The upper consolute point or cold cataract temperature, T_c, is the highest temperature at which the two phases can coexist. Below T_c, the cytoplasm segregates into a protein-rich phase and a water-rich phase. This temperature is species dependent and is very sensitive to age. The striking similarity between a ''normal'' aqueous two-phase system and cold cataracts serves as a motivation for this work in which we studied the interactions between the main proteins present in the eye lenses.

The cell lenses of all mammals are densely populated by a group of proteins known as crystallins. These proteins give the lenses the optical properties needed for vision. The three members of the family are α, β, and γ-crystallins. α-crystallins are highly polydispersed proteins which constitute 40% of the protein content of the lenses. β-crystallins are also polydispersed proteins whose molecular mass ranges from 50 000 to 300 000 and constitute 40% of the total protein in the lenses. Finally,

*Corresponding author. Tel.: +1-573-341-4427; fax: +1-573-341-4377.

E-mail address: forcinit@umr.edu (D. Forciniti)

0378-4347/00/$ – see front matter
PII: S0378-4347(00)00220-6

γ-crystallins are a heterogeneous group of low molecular mass proteins (~25 000) with subtle differences in their amino acid composition. It has been found that while the interactions between α-crystallins are repulsive, the interactions between γ-crystallins are attractive and this attraction decreases with increasing temperature [8,9]. Purified γ-crystallin fractions undergo a phase transition at slightly different temperatures. This difference in T_c between the various fractions permits the classification of them into low- and high-T_c groups. Since this phase transition is similar to that observed in whole lenses, γ-crystallins are considered model proteins for the study of cold cataracts.

In cold cataracts, as in aqueous two-phase systems, the dominant chemical species (in mass) is water. Unfortunately, the effect of solvent in the origin of the phenomenon has been overlooked. For example, Vérétout et al. [9] performed a small angle X-ray scattering of γ- and β-crystallins and showed, by fitting the experimental data with the renormalized mean spherical approximation, that interactions between γ-crystallins are attractive whereas interactions between β-crystallins are repulsive. However, the origin of the force remained obscure. A small-angle neutron scattering study of γII-crystallins published by us a few years ago [10] confirmed that the interaction between γII-crystallins is attractive (at their isoelectric point). The interpretation of those results was also based on the mean spherical approximation. The renormalized mean spherical approximation, as any other mean field approximation, accounts for solvent effects only through the dielectric constant of the solvent. Therefore, only limited information can be obtained from it if the experimental conditions are not carefully selected.

To test the validity of mean field theories to explain the phase transition that occurs when the cytoplasm splits into two phases or when they are used to model conventional aqueous two-phase systems and the distribution of proteins between the equilibrated phases, we have conducted a series of experiments using various crystallins fractions. In these experiments, we varied the chemical composition of the solvent (water) by adding either a structure-making species (glycerol) or a structure-breaker one (methanol). Since these two cosolvents have the same effect on dispersion and Coulombic forces but have an opposite effect on solvent mediated forces (such as attractive hydrophobic interactions or repulsive hydration forces), we are able to isolate the latter forces from the former ones. Two different techniques were used: small-angle neutron scattering (SANS) and dynamic light scattering (DLS). Our results show that solvent mediated forces cannot be neglected. We suggest that existing theories (including some Monte Carlo simulations available), although successful in explaining some experimental trends, fail to capture the complex interactions between these proteins in solution and the mechanisms of protein partitioning in aqueous two-phase systems because they do no account for the molecularity of the solvent.

2. Experimental

2.1. Materials

One-week-old calf lenses with individual masses of approximately 1 g were obtained from Antech Animal Technologies, (Tyler, TX, USA). All the other chemicals were analytical grade.

2.2. Methods

2.2.1. Preparation of samples

The total monomeric γ-crystallin fraction was separated from the α- and β-crystallins present in the centrifuged (1 h at 21 000 *g*) lens homogenate [3,7] using a 2.5×120 cm Sephadex G-75 column according to the procedure of Björk [11]. The separated γ-crystallin fraction was fractionated into γI-, γs-, γII-, γIII-, and γIV-crystallin using Slingsby and Croft's [7] modified Björk procedure [12], except that a larger column (2.5×50 cm), elution volume, and a series of linear salt gradients (instead of one linear salt gradient) were used.

The resulting fractions were desalted by exhaustive dialysis or by diafiltration using an Amicon PM10 disc membrane. The proteins were stored in a pH 5, 275 m*M* NaOAc buffer with 1 m*M* 2-mercaptoethanol at −60°C until needed. Five to ten μl samples of protein solution (~5 mg/ml) were isoelectrofocused, IEF, to determine their purity.

The proteins were dialyzed against nanopure water

(Barnstead Nanopure bioresearch deionization system) and lyophilized before traveling to the SANS facility. The purified proteins were dissolved in 99.9% D_2O or in mixtures of D_2O and fully deuterated methanol or glycerol and placed in flat cylindrical quartz cells having 1 mm thick circular windows and path lengths of 2 mm. The pH was adjusted to 5 with acetate buffer. Prior to carrying out the SANS experiments, the solutions were centrifuged at 6000 *g* for 15 min to remove any insoluble fractions. Protein concentrations after centrifugation were determined spectrophotometrically using an extinction coefficient of $A_{280\ nm}^{0.1\ wt\%}=2.18\ cm^2/mg$ for γII-crystallins. Multiple samples were mounted on an automatic rotating sample changer maintained at constant temperature by circulating water. To prevent the deuterated water from becoming contaminated with atmospheric moisture, all SANS samples remained sealed throughout the experiments.

2.2.2. Data collection

The experiments were performed on the W.C. Koehler 30 m SANS facility at the Oak Ridge National Laboratory [13]. The neutron wavelength (λ) was 0.475 nm ($\Delta\lambda/\lambda=5\%$) and the source (3.5 cm in diameter) and sample (1.0 cm in diameter) slits (irises) were separated by a distance of 7.5 m. The sample-detector distance was either 8.1 or 2.576 m and the data were corrected for instrumental backgrounds and detector efficiency on a cell-by-cell basis before radial averaging to give a *Q*-range (*Q* is the Bragg wave vector of the scattering), of $0.1<Q<2.4\ nm^{-1}$. The coherent intensities of the sample were obtained by subtracting the intensities of the corresponding blanks, which formed only a minor correction (<10%) to the sample data. The net intensities were converted to an absolute (±5%) differential cross section per unit sample volume (in units of cm^{-1}) by comparison with pre-calibrated secondary standards, based on the measurement of beam flux, vanadium incoherent cross section, the scattering from water and other reference materials [14]. The efficient calibration was based on the scattering from light water and this led to angle-independent scattering for vanadium, H-polymer blanks and water samples of different thickness in the range 1–10 mm.

The transmission of the sample was measured in a separate experiment [15] by collimating the beam with slits (irises) approximately 1 cm in diameter, separated by a distance ~7.5 m. A strongly scattering sample, porous carbon, was placed at the sample position to spread the beam over the whole detector, placed at a sample-detector distance ~10 m. Without the carbon in position, the beam would either be blocked by the beam stop or concentrated in a few detector cells, with the possibility of saturating or damaging the detector. The total count summed over the whole detector ($>10^5$) was recorded in a time period ~1 min and the sample being measured was placed over the slit, thus attenuating the beam. The count was repeated over the same time interval and the transmission is given by the ratio of the two counts after minor corrections (<0.1%) for the beam-blocked background due to electronic noise, cosmic rays, etc. In this geometry only scattering from the sample at *Q*-values $<10^{-2}\ nm^{-1}$ can enter the second iris and be scattered by the porous carbon and hence be counted by the detector.

The DLS experiments were performed on a fiber-optic quasi-elastic light scattering (FOQELS) instrument from Brookhaven Instruments (Brookhaven). The FOQELS uses an 800 nm solid state laser (70 mW) with a fixed scattering angle of 155° and a digital auto-correlator. The delay time intervals are not linearly spaced which allows broad distributions to be sampled properly. The sample was placed in a standard 4.5 ml rectangular plastic cuvette placed inside a constant temperature holder which is capable of controling the temperature in the range 5–75°C in steps of 0.1°C. The temperature was fixed at 23.9°C for all measurements. The method of cumulants was used to analyze the data. Particle size can be related to the diffusivity, D, for simple common shapes like a sphere, ellipsoid, cylinder and random coil. For a uniform sphere, the Stokes-Einstein relation is

$$D=\frac{kT}{3\pi\eta D_h} \quad (1)$$

where *k* is Boltzmann's constant, *T* is the temperature, η is the viscosity of the liquid in which the particle is moving and D_h is the hydrodynamic diameter. Eq. (1) assumes that the particles are moving independently of one another. When a distribution of sizes is present, the effective diameter

can be obtained by averaging the intensity-weighted diameters. In FOQELS, a multi-modal size distribution (MSD) analysis is available through the non-negatively constrained least squares (NNLS) approach developed by Grabowski and Morrison [16].

2.2.3. Sample preparation for DLS experiments

Nanopure water was used in all the experiments. Before each experiment, the buffers were filtered through a Whatman 0.45 μm polysulfone membrane filter. Because the solutions used in the DLS particle size measurements need to be very clean and dust-free, these filtered solutions were filtered again through a Whatman 0.2 μm polyethersulfone membrane filter. The proteins were dissolved in this water and the prepared solutions were filtered through a MSI 0.1 μm nylon membrane filter before each measurement.

2.3. Data analysis

The analysis of SANS data is well documented in the literature [17–19] and the reader is referred to it for additional details. We limit our presentation here to a few topics to facilitate the discussion of our results. In small-angle neutron scattering experiments, the sample is illuminated with a beam of cold neutrons. The neutrons (waves) interact with the nuclei of the sample and the resulting diffracted spherical waves generate a complex interference pattern. The intensity of the scattered beam (the sum of the squares of the amplitudes of the waves) is the experimentally accessible quantity, $I(Q)$. $I(Q)$ can be written in terms of intraparticle interferences ($P(Q)$) and interparticle interferences ($S(Q)$). For monodisperse samples, $I(Q)$ is given by:

$$I(Q) = nP(Q)\left[1 + \left(\frac{\langle F(Q)\rangle^2}{\langle F(Q)^2\rangle}\right)[S(Q) - 1]\right] \quad (2)$$

where $P(Q)$ is given by:

$$P(Q) = \left[\frac{\sum_i b_i + f_{H/D}H_{ex}(b_D - b_H)}{V_p} - \rho_s\right]^2 \langle F(Q)^2\rangle \quad (3)$$

In Eqs. (2) and (3), $P(Q)$, $S(Q)$, and n are the intra- and interparticle structure factors, and the number density of the particles in the sample, respectively. $F(Q)$ is the form factor, ρ_s is the mean coherent scattering length density of the solvent (6.34×10^{10} cm^{-2} for 99.9% D_2O), Σb_i is the sum of the scattering lengths of all the atoms in the native protein ($513.95\cdot10^{-12}$ cm, from the amino acid sequence of γ-crystallins), $f_{H/D}$ is the fraction of the labile protons that are accessible to the solvent (usually taken as 0.8 for proteins in pure D_2O), $H_{ex}=347.5$ (from the amino acid sequence of γ-crystallins) is the total labile hydrogen atoms, b_D, b_H, and b_{D_2O} are the neutron scattering lengths of deuterium, hydrogen, and ''heavy'' water respectively, and V_p is the protein volume. The first term inside the bracket is, therefore, the scattering density of the protein (ρ_p) and the difference between ρ_p and ρ_s is called the contrast.

If the appropriate experimental conditions are selected, inter- and intraparticle interactions can be uncoupled. For example, for weakly interacting systems interparticle correlations are negligible ($S(Q)\sim1$) and the intensity is given by

$$I(Q) = nP(Q) \quad (4)$$

The form factor can be calculated from the crystal structure of the protein, by modeling the proteins as an assembly of spheres [21], or by assuming a shape for the protein molecule [19]. In this work, γ-crystallins were modeled as prolate ellipsoid of dimensions $a=43.8$; $b=c=12.5$ Å [10].

The intermolecular structure factor at zero momentum transfer, $S(Q=0)$, is proportional to the isothermal compressibility. Therefore, it diverges at the spinodal and at the critical point. $S(Q)$ is proportional to the Fourier transform of the pair correlation function, $g(r)$. $\rho g(r)\ 4pr^2\ dr$ is the number of molecules between r and $r+dr$ about a central molecule (ρ is the bulk density). Therefore, the local density, $\rho(r)$, is given by,

$$\rho(r) = g(r)\rho \quad (5)$$

One approximation used to calculate $g(r)$ and therefore $S(Q)$ is the mean spherical approximation. The mean spherical approximation is a closure of the Ornstein-Zernike equation which can be understood as a balance of correlation functions, i.e.,

{Total Correlation} = {Direct Correlation} + {Indirect Correlations}

or

$$h(r_{12}) = c(r_{12}) + \rho \int c(r_{13})h(r_{23})\,dr_3 \quad (6)$$

where $h(r_{12})$ is the total correlation function $(g(r_{12}) - 1)$ and $c(r_{13})$ is the direct correlation function. The mean spherical approximation assumes that,

$$\begin{aligned} g(r) &= 0 \qquad r < \sigma \\ c(r) &= -\beta u(r) \quad r > \sigma \end{aligned} \quad (7)$$

where $\beta = 1/kT$, σ is the hard core diameter of the molecules, and $u(r)$ is intermolecular potential. This set of equations can be solved analytically to yield the Fourier transform of $g(r)$, $S(Q)$.

The interparticle structure factor, $S(Q)$, is calculated here using the mean spherical approximation (MSA) for a hard-core potential of diameter σ plus a Sutherland-type of attractive tail. We have chosen the MSA instead of more precise liquid-state theories because of its relative simplicity. The insensitivity of liquid state theories to small changes in the shape of the pair potential is a disadvantage of SANS coupled with liquid state theories because equally good fittings can be obtained using slightly different sets of parameters [22]. Whereas these observations are important in the analysis of interactions between moderated size ions, they are less important for macroions (e.g. proteins). In addition, the insensitivity of liquid state theories to the real shape of the potential makes unnecessary the use of more refined theories beyond the MSA.

The pair potential was taken as

$$u(r) = \infty \quad r < \sigma \quad (8a)$$

and

$$u(r) = \gamma \exp\left(\frac{k - x}{x}\right) \quad (8b)$$

where, $x = r/\sigma$, σ is the diameter of the scatters (if they are not spherical σ is the diameter of the equivalent sphere), γ is the potential at $x = 1$ and $k = \sigma\kappa$ with κ equal to the inverse of the van der Waals diameter (2.9 Å) of a water molecule. Chen and Bendedouch [19] used this empirical approach successfully to fit SANS data for BSA near its isoelectric point.

Inter- and intraparticle structure factors were calculated using a FORTRAN code. For the calculation of the interparticle structure factor, the code solves the Ornstein–Zernike equation in the MSA according to Hayter and Penfold [23]. The code which calculates $S(Q)$ and $P(Q)$ was combined with the IMSL nonlinear regression program DRNLIN [24] to regress the data. As mentioned previously, equally good fittings can be obtained using different sets of parameters; so, we proceeded as follows. The data was fitted using different initial guesses. The sums of the square of the errors associated with the fitting parameters for each initial guess were compared and the fit with the least sums of squared error was chosen as the best global fit.

Reproducing the results of Hayter and Penfold [23] validated the MSA code (interparticle structure factor). The original set of equations was rearranged to avoid rounding errors that caused numerical problems. A key step in Hayter and Penfold's algorithm is to find the physically meaningful root of a fourth degree polynomial. Often, the calculations involve subtraction of very similar but large numbers; so, if the equations are not rearranged, the physically sound root cannot be found. Reproducing the result obtained by Bendedouch and Chen (inter- and intraparticle structure factors) validated our fitting code for BSA [20].

3. Results and discussion

3.1. γII-crystallins

The SANS experimental data for this protein could not be fitted with positive contact potentials, γ; this indicates that the net intermolecular forces between γII-crystallins are attractive – in agreement with the results of Tardieu et al. [8], Fine et al. [25], and Lomakin et al. [26]. Thus, the data for each concentration, solvent composition, and temperature was fitted with two parameters, γ and the intensity correction factor. The intensity data correction factor is used because the experimental scattered intensity did not approach zero at high *Q*s as it should for a uniform rigid particle. Chen and Bendedouch used a

similar intensity data correction factor in their work with BSA [19]. However, our use of the correction factor is slightly different. We used the data correction as a parameter in the fitting program, which simply subtracted the height intensity from each spectrum as a flat background. The data correction is small in most cases, but it becomes more significant at higher protein concentration.

3.2. Effect of temperature

The scattered intensity versus momentum transfer data at two temperatures is shown in Fig. 1. The intermolecular structure factors used to fit the data are shown in the inset of the same figure and the contact potential is plotted as a function of temperature in Fig. 2 (open circles). The intermolecular

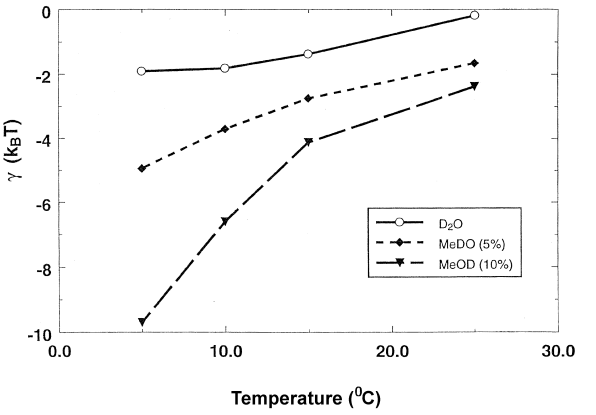

Fig. 2. Plot of the contact potential versus temperature for γ-crystallins in pure D_2O, 5% methanol and 10% methanol. Protein concentrations range from 27.3 to 34.2 mg/ml.

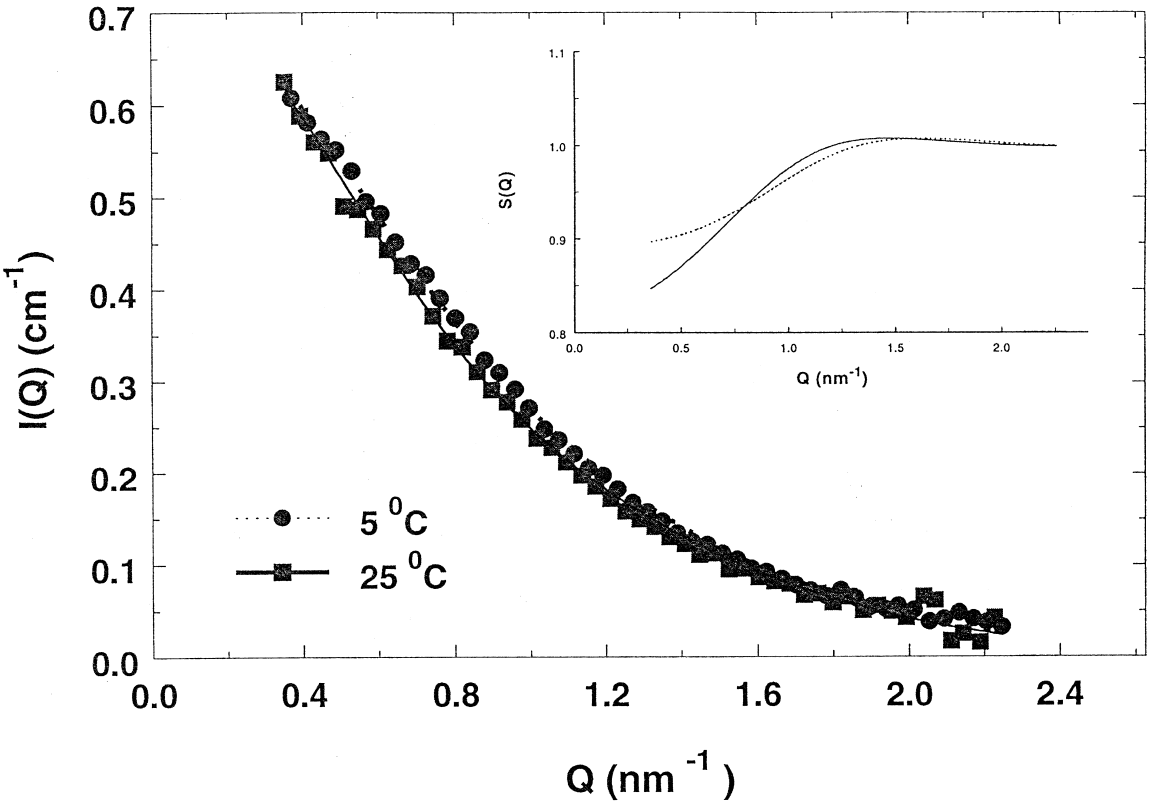

Fig. 1. Scattering intensity versus momentum transfer for γ crystallins at two temperatures. The pH is 5 and the protein concentration is 31.2 mg/ml. The symbols are the experimental data and the lines the best fits. The inset shows the calculated structure factors.

structure factor ($S(Q)$) is practically equal to 1 except at very low Q-values where it becomes smaller than one. The absence of a first correlation peak in $S(Q)$ indicates that the interactions between these proteins are short-ranged. Fig. 2 shows that the absolute value of the contact potential linearly increases with decreasing temperature. This is in agreement with Lomakin et al. [26] who postulated that the depth of the well of a square-well potential follows a similar trend with temperature. They needed to use this temperature dependence for their Monte Carlo simulations to agree with experimental phase diagrams of crystallins.

3.3. Effect of methanol

Fig. 3 shows the experimental and calculated scattered intensity versus the momentum transfer with and without added methanol at 5°C. Note that the effect of small differences in protein concentration is ignored in the discussion that follows. This is possible because in this range of protein concentrations the values of the fitting parameters change slightly upon small changes in protein concentration. The extracted intermolecular structure factors are different from those shown in Fig. 1. The addition of methanol produces a pronounced valley at $Q \sim 1$ nm^{-1} and the value of $S(Q \rightarrow 0)$ increases sharply. This increase in $S(Q \rightarrow 0)$ upon addition of methanol means that the isothermal compressibility is increasing. Recall that the isothermal compressibility becomes infinite at the spinodal (the onset of a phase separation) or at the critical point. The contact potential at two different methanol concentrations is plotted versus temperature in Fig. 2 (filled symbols). The addition of methanol (even moderate

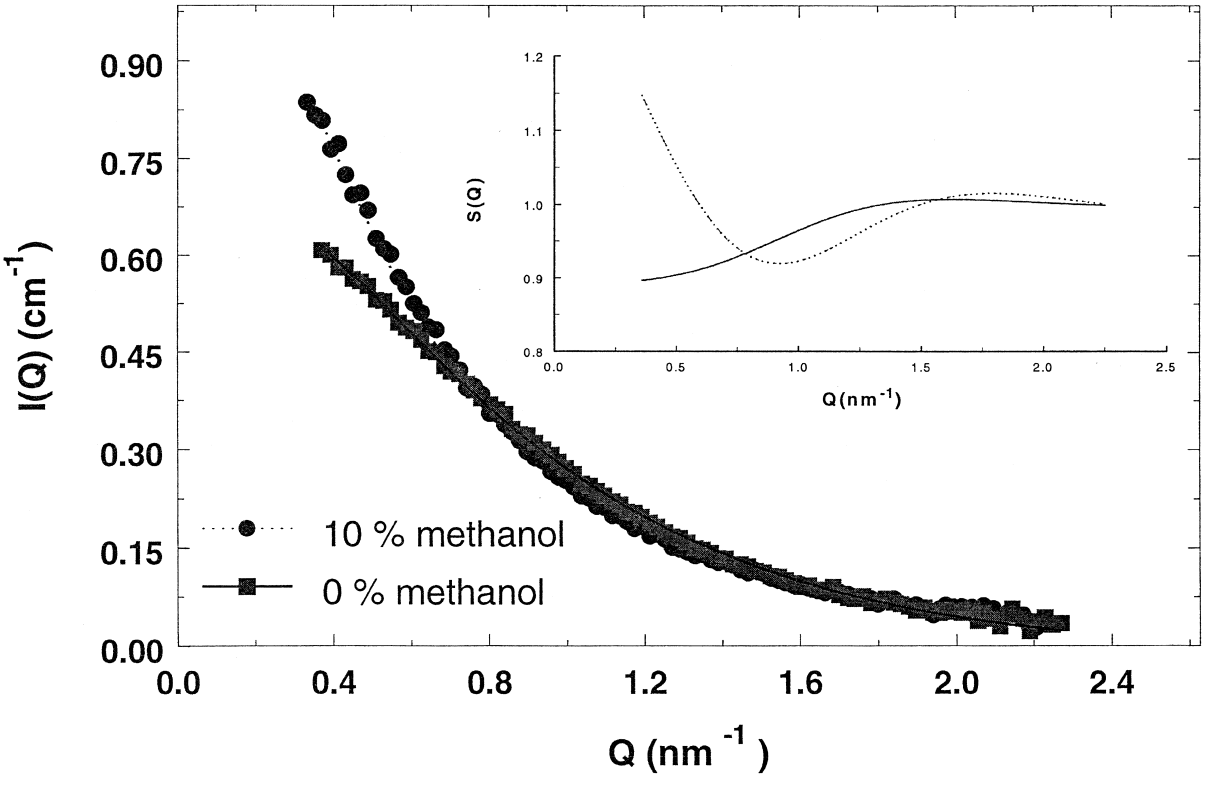

Fig. 3. Scattering intensity versus momentum transfer for γ-crystallins with and without the addition of methanol. The symbols are the experimental data and the lines the best fits. The pH is 5 and the temperature 5°C. The protein concentrations are 31.2 mg/ml (in water) and 27.3 mg/ml (in 10% methanol). The symbols are the experimental data and the lines the best fits. The inset shows the calculated structure factors.

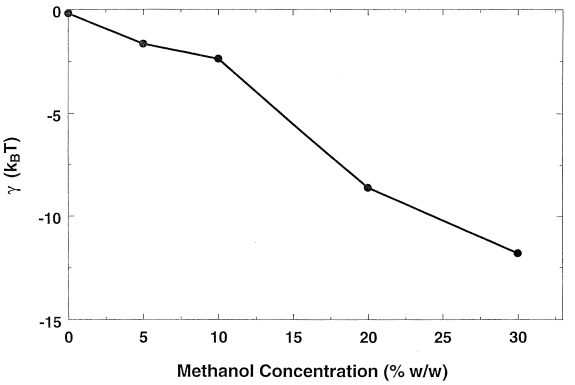

Fig. 4. Contact potential, γ, versus methanol concentration at 25°C and pH=5. The protein concentration ranges from 27.3 to 34.2 mg/ml. The line is drawn to guide the reader's eye.

amounts) makes the temperature dependence of γ non-linear. There is a drastic increase in the absolute value of γ at low temperatures and high methanol concentrations. The values of the contact potential are plotted versus the concentration of methanol in Fig. 4. Clearly, a nonlinear relation exists between the strength of the attraction and the concentration of methanol. The same nonlinear relation is observed for the effect of ethanol on hydrophobic interactions [27]. Although this maybe just a coincidence, it demonstrates that the effect of adding a cosolvent on the potential is not simple and that the linear dependence between the potential energy and temperature cannot be deemed as universal.

Fig. 5 shows the calculated intermolecular potential used to fit the data (Eq. (8)). Two observations can be readily made. First, the potential is short-ranged and extends for only one or two molecular diameters. So, long range order for this group of crystallins is nonexistent. Second, the pair potential for this protein in water is very close to a hard sphere potential ($\gamma=0$) Also, the range and the strength of the potential increases with decreasing temperature as well as upon addition of methanol. This makes the effect of methanol more noticeable at the lowest temperatures. These results suggest that as the temperature decreases the correlation between molecules becomes more long-ranged and it will become infinitely long-ranged at the critical point. This is consistent with the fact that these proteins exhibit an upper consolute point.

The addition of methanol to an aqueous solution has various effects on the intermolecular forces. The addition of methanol decreases the dielectric constant of water; thus, it increases the strength of Coulombic repulsions/attractions and dispersion forces. Tilton et al. [28] reported that methanol decreases lyophilic interactions in ribonuclease solutions. They argued that the disruption of the hydrogen bonding mesh by methanol breaks the water structure and therefore makes water more hydrophobic. Therefore, the addi-

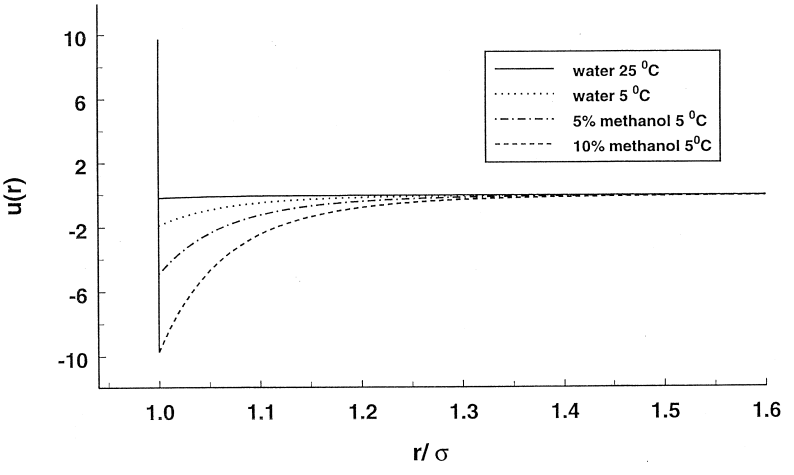

Fig. 5. Intermolecular potential as a function of distance.

tion of methanol to an aqueous solution decreases hydrophobic interactions between the solutes [27]. Finally, the addition of methanol to an aqueous solution disrupts the well-organized layers of water that surround a protein molecule. This layer of water originates another solvent mediated force, hydration force, which is the result of the repulsions between water layers from different molecules. Because of their nature, hydration forces are short-ranged. At pH 5 these proteins are positively charged. Therefore, the addition of methanol will increase Coulombic repulsions and its addition should also weaken hydrophobic attractions. Therefore, the addition of methanol increases attractions because it increases dispersion forces (attractive) and decreases hydration (repulsive) forces.

3.4. β-crystallins

The spectra for these proteins (Fig. 6) are completely different from the ones observed with γ-crystallins (Fig. 1). A strong interaction peak is clearly noticeable at $Q=0.2\sim0.3$ nm^{-1}. The figure also shows that the intensity at low values of Q decreases as the concentration of the proteins increases, as it should be for a solution where repulsive interactions dominate. The addition of methanol and glycerol yields some puzzling results.

Special care must be taken to interpret the results shown in Fig. 6 since a mixture of α and β crystallins is highly polydisperse. We analyzed the polydispersity of these proteins by dynamic light scattering. The histogram presented in Fig. 7 shows that three main molecular sizes dominate the scattering. The first one is centered at around 8 nm and corresponds to β-crystallins. The second one is centered at around 20 nm and must correspond to α-crystallins. The last one is centered at 140 nm and must correspond to large aggregates of α and/or β crystallins. Delaye et al. [29] observed a similar distribution of sizes except that only two populations were observed (one with an average size of 10 nm and another with an average size of 150 nm). Actually, their data interpretation begins with the assumption that they have two different populations that our data clearly shows is not correct.

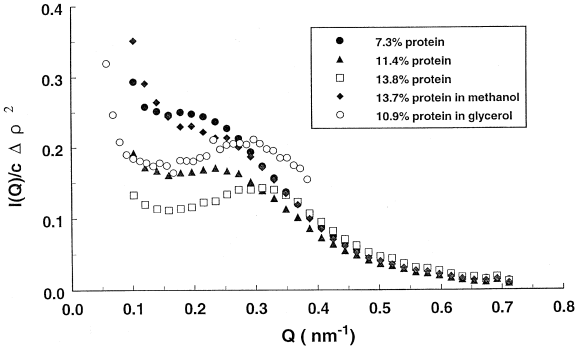

Fig. 6. Scattering intensity versus momentum transfer for α and β crystallins with and without the addition of methanol and glycerol. Temperature: 25°C. The protein concentrations are indicated in the figure. The intensity has been divided by protein concentration and by the square of the contrast to highlight the effect of the cosolvents on $S(Q)$.

Tardieu et al. and Vérétout et al. [8,9] conducted X-ray small angle scattering experiments with α and β crystallins but they ignored the polydispersity of their preparation in their analysis. Our dynamic light scattering studies clearly indicate the polydispersity cannot be ignored. We believe that the interaction peak that we observed in Fig. 6 can be assigned to the smaller proteins (β-crystallins) whereas the interaction peak for α-crystallins occurs at such a small angle that cannot be reached by the instrument. The polydispersity of the sample makes impossible to try to fit the data with Eq. (2). Therefore, we limit our analysis to some qualitative discussions. The first interaction peak should move to higher Qs as the concentration of the scatters increases and/or as the strength of repulsive forces increases. For example, the first interaction peak moves to higher Q values as the charge in colloidal systems increases [23]. This trend is also observed here (compare the spectra in pure water at the three protein concentrations). We have plotted the position of the first interaction peak versus the mean distance between the scatters, $c^{-1/3}$, (where c is the protein concentration in units of mg/ml) in Fig. 8. As a first approximation, the position of the peak should correlate with the inverse of the mean distance between the scatters. The figure shows that in the presence of methanol the scatters are further apart from each other (the stronger attractive force produces small aggregates) whereas in the presence of glycerol the scatters seem to be closer to each other. This is equivalent to an increase in repulsions in the presence of glycerol (aggregates

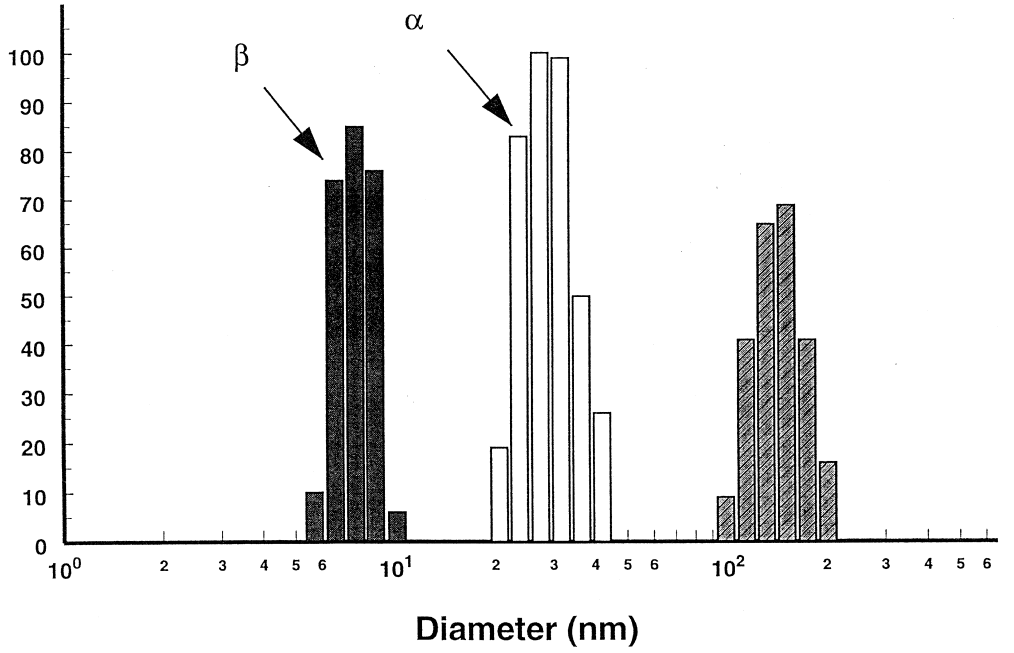

Fig. 7. The histogram shows the distribution of species according to size in the αβ crystallins preparation.

are not formed) and an increase in attractions in the presence of the mono alcohol (aggregates are formed). Both solvents decrease the dielectric constant of water; therefore, the two solvents will similarly affect Coulombic and dispersion forces. However, these two solvents have opposite effects on hydrophobic interactions. Methanol decreases hydrophobic attractions whereas glycerol increases them. Our data shows that the addition of methanol increases attractions but the addition of glycerol increases repulsions. Therefore, hydrophobic or electrostatic forces cannot be invoked to explain the observed trends. We believe that, the effect of these two solvents on hydration forces can be used to explain the experimental observations. The addition of methanol to a protein solution disrupts the hydration layer and thus decreases the strength of the repulsions between those water layers. Glycerol, on the contrary, preferentially hydrates proteins. Therefore, the addition of this solvent to a protein solution will increase the repulsion between hydration layers.

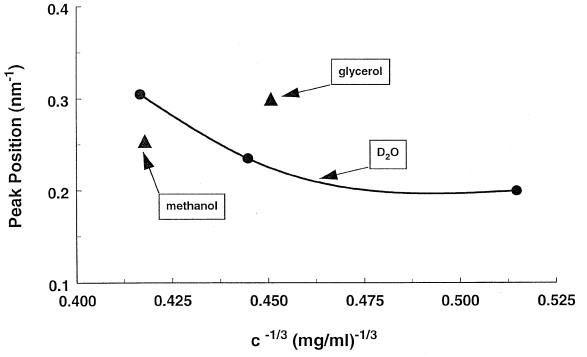

Fig. 8. Plot of the position of the first interference peak versus $c^{-1/3}$.

Clearly, our data shows that the distinctive solution properties of crystallins are a consequence of a delicate balance in intermolecular forces. We would like to expand this point further. Often, a very limited amount of information is used to reach conclusions about intermolecular potentials of complex molecules. This is particularly risky when working with proteins because proteins are so complex that limited information may lead to a wrong physical description. On the contrary, an expanded set of data designed on physically sound theories

provides enough information to infer the correct physical picture.

Acknowledgements

The work at UMR was supported by the University of Missouri Research Board. The research at Oak Ridge supported by the Division of Materials Sciences, U.S. Department of Energy under contract No. DE-AC05-96OR22464 with Lockheed Martin Energy Research Corp. We also like to thank to Drs. R. Triolo and G. Wingall for helping us performing the SANS experiments.

References

[1] P.Å. Albertsson, Partition of Cell Particles and Macromolecules, 3rd ed., Wiley (Interscience), New York, 1986.
[2] V.G. Taratuta, A. Holschbach, G.M. Thurston, D. Blankschetein, G.B. Benedek, J. Phys. Chem. 94 (1990) 2140.
[3] O.J.A. Thomson, P. Schurtenmberger, G.M. Thurston, G.B. Benedek, Proc. Natl. Acad. Sci. USA 84 (1987) 7079.
[4] J.I. Clark, G.B. Benedek, Inves. Ophthalmol. Vis. Sci. 19 (1980) 771.
[5] P. Hammer, G.B. Benedek, Curr. Eye Res. 2 (1982/1983) 809.
[6] R.J. Siezen, M.R. Fisch, C. Slingsby, G.B. Benedek, Proc. Natl. Acad. Sci. 82 (1985) 1701.
[7] C. Slingsby, L.R. Croft, Exp. Eye Res. 17 (1973) 369.
[8] A. Tardieu, F. Vérétout, B. Krop, C. Slingsby, Eur. Biophys. J. 21 (1992) 1.
[9] F. Vérétout, M. Delaye, A. Tardieu, J. Mol. Biol. 205 (1989) 713.
[10] P. Petitt, M. Edwards, D. Forciniti, Eur. J. Biochem. 243 (1997) 415.
[11] I. Björk, Exp. Eye Res. 1 (1961) 145.
[12] I. Björk, Exp. Eye Res. 3 (1964) 254.
[13] W.C. Koehler, Physica (Utrecht) 137B (1986) 320.
[14] G.D. Wignall, F.S. Bates, J. Appl. Cryst. 20 (1986) 28.
[15] W.S. Dubner, J.M. Schultz, G.D. Wignall, J. Appl. Cryst. 23 (1990) 469.
[16] E. Grabowski, I. Morrison, in: B.E. Dahneke (Ed.), Measurements of Suspended Particles By Quasi-elastic Light Scattering, Wiley, New York, 1983, p. 199.
[17] A. Guinier, G. Fournet, Small Angle Scattering of X-rays, Wiley, New York, 1955.
[18] B. Jacrot, Rep. Prog. Phys. 39 (1976) 911.
[19] S.-H. Chen, D. Bendedouch, Methods in Enz. 130 (1986) 79.
[20] D. Bendedouch, S.H. Chen, J. Phys. Chem. 88 (1984) 648.
[21] S.J. Perkins, in: C. Jones, B. Mulloy, A.H. Thomas (Eds.), Methods in Molecular Biology, 1994, p. 39.
[22] D.M. Duh, A.D.J. Haymet, J. Chem. Phys. 100 (1994) 2244.
[23] J.B. Hayter, J. Penfold, Mol. Phys. 42 (1981) 109.
[24] IMSL, Inc., IMSL STAT/LIBRARY: FORTRAN Subroutines for Statistical Analysis. 1989. IMSL, Houston, TX.
[25] B.M. Fine, A. Lomakin, O.O. Ogun, G.B. Benedek, J. Chem. Phys. 104 (1996) 326.
[26] A. Lomakin, N. Asherie, G.B. Benedek, J. Chem. Phys. 104 (1996) 1646.
[27] A. Ben-Naim, Hydrophobic Interactions, Plenum press, New York, 1980.
[28] R.D. Tilton, C.R. Robertson, A.P. Gast, Langmuir 7 (1991) 2710.
[29] M. Delaye, J.I. Clark, G.B. Benedek, Biophys. J. 37 (1982) 647.